Estimation of Mobile Speed and Average Received Power in Wireless Systems Using Best Basis Methods

Ravi Narasimhan, *Member, IEEE,* and Donald C. Cox, *Fellow, IEEE*

***Abstract*—A new method is presented for estimating the mobile speed and the average received power in general wireless propagation environments. The locally stationary received signal is expanded in a local exponential basis using best basis methods of wavelet analysis. An estimate of the time-varying Doppler power spectrum is obtained together with an estimate of the maximum Doppler frequency, which is proportional to the mobile speed. The average received power is then estimated by integrating the time-varying spectrum. Simulations demonstrate good tracking of variable mobile speed and average received power for a wide range of angular distributions of incident power. The estimator is shown to perform significantly better than an adaptive averaging method described in the literature. The speed and average power estimates are also used to detect the corner effect in urban cellular systems to improve handoff performance and reduce the call dropping rate.**

***Index Terms*—Speed estimation, wavelets, wireless communication.**

I. Introduction

ESTIMATES of the mobile speed and the average received power in wireless communication systems are useful for several purposes. Mobile speed can be used to improve system control algorithms such as handoff or channel assignment. For example, mobile speed can be used to determine whether a mobile station which requests access to the wireless system should be assigned to a microcell (for low speeds) or to an umbrella macrocell (for high speeds). Accurate estimates of the average received power also improve the performance of handoff, power control, and channel assignment algorithms and, thereby, increase the realized system capacity.

In many environments, the received signal consists of a sum of waves that have been reflected by objects such as mountains, trees and buildings. The sum of many waves at the receiver gives rise to small-scale spatial variation of the received envelope (on the order of a wavelength). In situations where there is no dominant path between the base station and the mobile station, the small-scale spatial variation is called Rayleigh fading [1]. The received signal is nonstationary for distances on the order of building sizes since the mean of the small-scale variation changes considerably. This large-scale variation of the mean is known as shadowing. The mean of the shadowing also decreases as the distance between the base station and the mobile station increases.

Estimates of the mobile speed can be obtained by using the statistics of the received signal. For example, level crossing rates [2] or the autocovariance [3] of the received envelope have been used to estimate speed. Speed estimates have also been obtained by estimating the maximum Doppler frequency using eigenspace methods [4] and spectrum estimation methods [5]. These methods are designed under specific assumptions of the angular distribution of incident power. Another method of velocity estimation requires knowledge of the average signal strength for all locations within a region of interest and uses a technique similar to the multidimensional scaling (MDS) method of statistical data analysis [6]. All of the above techniques require estimates of the average signal power, and some methods also require the signal autocorrelation. A difficulty in obtaining such estimates is the nonstationary nature of the received signal. An appropriate window which depends on the unknown mobile speed must be chosen to estimate the required quantities.

The average received power is the local mean of the small-scale variation (up to a constant) and represents the distance-dependent trend and shadowing. The most widely used estimate of average power is the average of samples of the received envelope (or logarithm of the envelope) taken at a constant temporal interval. In [7], the bandwidth of a continuous-time lowpass filter is chosen to minimize the estimation error for a nominal constant mobile speed. In [8], estimates of the average power are obtained using a spatial analog averaging filter; in addition, the number of uncorrelated samples needed for discrete-time averaging is determined under the assumption that signal samples taken at a constant spatial interval are available. Another paper [9] derives the minimum-variance unbiased estimator for the average power under the assumption that all samples used in the estimate have the same mean and are uncorrelated. Since in [9] the samples must be taken at a constant temporal interval, the assumption places constraints on the unknown and possibly time-varying mobile speed. An adaptive method to estimate the average power is proposed in [3] where the squared deviations of the logarithm of the received envelope are used to estimate the maximum Doppler frequency. The maximum Doppler frequency is then used to adapt the number of signal samples that are averaged to estimate the signal power. This method assumes Rayleigh fading with a uniform angular distribution of incident power in a plane.

The literature mentioned above has considered only the problem of a constant, unknown mobile speed. For variable

Paper approved by R. A. Valenzuela, the Editor for Transmission Systems of the IEEE Communications Society. Manuscript received December 22, 1999; revised July 12, 2000 and March 22, 2001. This work was supported by a National Science Foundation Graduate Research Fellowship.

R. Narasimhan is with the Department of Electrical Engineering, Stanford University, Stanford, CA 94305 USA, and also with Marvell Semiconductor, Inc., Sunnyvale, CA 94085 USA (e-mail: nkravi@wireless.standford.edu).

D. C. Cox is with the STAR Laboratory, Department of Electrical Engineering, Stanford University, Stanford, CA 94305 USA (e-mail: dcox@spark.stanford.edu).

Publisher Item Identifier S 0090-6778(01)10615-X.

speeds, the duration of the observation window must be constantly adapted, and the rate of adaptation will be critical to the performance of the speed and average power estimators. In particular, errors in the estimates could propagate due to suboptimal observation windows. Recently, a speed estimator has been introduced which tracks variable mobile speed without requiring knowledge of the average received power [10]. Another recent paper [11] provides a method of estimating the average received power without requiring estimates of the variable mobile speed. While the techniques described in [10], [11] overcome the restrictions of a constant mobile speed, these methods, like all the others in the literature, assume Rayleigh fading with a uniform angular distribution of incident power in a plane.

This paper describes a new method of estimating the mobile speed and the average received power. The method uses the local stationarity of the received signal and does not assume a specific angular distribution of incident power. The signal is expanded in a basis of smooth local complex exponentials using the best basis methods of [12], [13]. This technique automatically selects regions of approximate stationarity of the signal. Within each such region, an estimate of the time-varying Doppler spectrum is obtained. The time-varying spectrum yields estimates of the mobile speed and the average received power as a function of time. These estimates are then applied to the detection of the corner effect in urban cellular systems. The corner effect refers to a sudden change in the average received power when a mobile station makes a turn at an intersection. Timely detection of the corner effect can initiate a handoff to a nearby base station to reduce the call dropping rate.

The paper is organized as follows. In Section II, wireless propagation and noise models are presented. Section III presents a method to estimate the time-varying spectrum, the mobile speed and the average received power using two antennas at the mobile station that are oriented along the mobile velocity. Section IV determines relevant parameters and presents performance results for variable mobile speeds, including a comparison with an extension of the adaptive averaging method described in [3]. A corner detection method which uses the speed and average power estimates is described in Section V. Section VI presents an extension of the speed and average power estimation technique using best basis methods to the case of an arbitrary orientation of the antennas at the mobile station. Section VII concludes the paper.

II. Wireless Propagation and Noise Models

A. Macrocellular Model

The propagation model discussed here takes into account three effects that are present in many macrocellular wireless environments: correlated multipath fading, correlated log-normal shadowing, and a distance-dependent trend [1]. The received bandpass signal at a mobile station consists of a sum of contributions from several paths. Let $r_c(\mathbf{x})$ denote the complex envelope of the received signal at mobile position $\mathbf{x}$. The signal $r_c(\mathbf{x})$ is an approximate wide-sense stationary complex Gaussian random process in a small neighborhood of $\mathbf{x}$. Let $s(\theta)$ denote the distribution of incident power in angle θ in a plane. For a transmitting base station located at $\mathbf{x_B}$, let $p(\mathbf{x}, \mathbf{x_B})$ be the received power at the mobile station averaged over a small neighborhood of $\mathbf{x}$. Let λ denote the carrier wavelength and

$$\mathbf{k}(\theta) = -\frac{2\pi}{\lambda}\begin{pmatrix}\cos\theta \\ \sin\theta\end{pmatrix} \tag{1}$$

represent an incident wave vector which makes an angle of θ with respect to the x-axis in a fixed rectangular coordinate system in the horizontal plane. From the above conditions and for an omnidirectional antenna, the autocorrelation of $r_c(\mathbf{x})$ for a mobile velocity in the direction $\mathbf{u}$ and for a small neighborhood of $\mathbf{x}$ can be written as

$$\begin{aligned} R_{r_c r_c}(y\mathbf{u}, p(\mathbf{x}, \mathbf{x_B})) &= \frac{1}{2} E\{r_c(\mathbf{x}+y\mathbf{u})\overline{r_c(\mathbf{x})}\} \\ &= p(\mathbf{x}, \mathbf{x_B}) \int_{-\pi}^{\pi} e^{-j\langle \mathbf{k}(\theta), y\mathbf{u}\rangle} s(\theta)\, d\theta \end{aligned} \tag{2}$$

where $\overline{r_c(\mathbf{x})}$ denotes the complex conjugate of $r_c(\mathbf{x})$ and $\langle \mathbf{k}(\theta), \mathbf{u}\rangle$ denotes the inner product between $\mathbf{k}(\theta)$ and $\mathbf{u}$. The autocorrelation (2) explicitly indicates the fact that $r_c(\mathbf{x})$ is locally stationary in a small neighborhood of $\mathbf{x}$. A model for $r_c(\mathbf{x})$ is then given by

$$r_c(\mathbf{x}) = \left[\frac{4\pi p(\mathbf{x}, \mathbf{x_B})}{N_{r_c}}\right]^{1/2} \sum_{n=0}^{N_{r_c}-1} [s(\theta_n)]^{1/2} e^{j[-\langle \mathbf{k}_n, \mathbf{x}\rangle + \phi_n]} \tag{3}$$

where N_{r_c} is the number of terms in the model, $\theta_n = -\pi + 2\pi n/N_{r_c}, \mathbf{k}_n = \mathbf{k}(\theta_n)$, and ϕ_n are uniform, independent and identically distributed (i.i.d.) random variables on $[-\pi, \pi)$. The autocorrelation of (3) approaches (2) as $N_{r_c} \to \infty$ since $p(\mathbf{x} + y\mathbf{u}, \mathbf{x_B}) \approx p(\mathbf{x}, \mathbf{x_B})$ for $|y|$ less than the correlation length of the shadowing.

The average received power $p(\mathbf{x}, \mathbf{x_B})$ contains the distance-dependent trend and log-normal shadowing [14]. Let γ represent the exponent of the distance-dependent trend. Furthermore, let $10^{L(\mathbf{x}, \mathbf{x_B})/10}$ denote the log-normal shadowing between the locations $\mathbf{x}$ and $\mathbf{x_B}$. The received power averaged over a neighborhood of $\mathbf{x}$ due to the base station located at $\mathbf{x_B}$ can then be expressed as

$$p(\mathbf{x}, \mathbf{x_B}) = P_0 \|\mathbf{x} - \mathbf{x_B}\|^{-\gamma} 10^{L(\mathbf{x}, \mathbf{x_B})/10} \tag{4}$$

where P_0 accounts for antenna parameters, transmitted power, and other relevant system parameters. The process $L(\mathbf{x}, \mathbf{x_B})$ is a zero-mean Gaussian random process that is wide-sense stationary in the variable $\mathbf{x}$. Let $R_{LL}(y\mathbf{u}, \mathbf{x_B})$ denote the autocorrelation of $L(\mathbf{x}, \mathbf{x_B})$ in the variable $\mathbf{x}$ along the direction $\mathbf{u}$. An empirical model for $R_{LL}(y\mathbf{u}, \mathbf{x_B})$ is [15]

$$R_{LL}(y\mathbf{u}, \mathbf{x_B}) = \sigma_L^2(\mathbf{x_B}) \exp\left(-\frac{|y|}{d_0(\mathbf{x_B})}\right) \tag{5}$$

where $\sigma_L^2(\mathbf{x_B})$ and $d_0(\mathbf{x_B})$ are the variance and correlation length of $L(\mathbf{x}, \mathbf{x_B})$, respectively. The power spectrum $S_{LL}(\nu, \mathbf{x_B})$ of $L(\mathbf{x}, \mathbf{x_B})$ is given by

$$S_{LL}(\nu, \mathbf{x_B}) = \frac{2d_0(\mathbf{x_B})\sigma_L^2(\mathbf{x_B})}{1 + [2\pi\nu d_0(\mathbf{x_B})]^2} \tag{6}$$

where ν denotes spatial frequency. The spectrum is truncated to a maximum spatial frequency of $\nu_{\max}$. Let $\tilde{D}$ be the distance

traveled by the mobile station within a time period of interest and define $D = \max(\tilde{D}, Jd_0)$ where $J \gg 1$. A model for the process $L(\mathbf{x}, \mathbf{x_B})$ can be shown to be

$$L(\mathbf{x}, \mathbf{x_B}) = \sum_{n=-N_L}^{N_L-1} \left[\frac{2}{CD} S_{LL}\left(\frac{(n+1/2)}{D}, \mathbf{x_B}\right)\right]^{1/2} \times \cos\left[\frac{2\pi\langle \mathbf{x}, \mathbf{u}\rangle}{D}(n+1/2) + \beta_n\right] \quad (7)$$

where

$$C = \frac{1}{D\sigma_L^2(\mathbf{x_B})} \sum_{n=-N_L}^{N_L-1} S_{LL}\left(\frac{(n+1/2)}{D}, \mathbf{x_B}\right)$$
$$\nu_{\max} = N_L/D \quad (8)$$

and β_n are uniform, i.i.d. random variables on $[-\pi, \pi)$. It can be shown that for fixed D, the autocorrelation of (7) approaches (5) as $N_L \to \infty$.

B. Microcellular Model

The microcellular model described here is used to evaluate the corner detection method of Section V. To simplify notation in this subsection, we let the position of the base station be the origin of coordinates, i.e., $\mathbf{x_B} = \mathbf{0}$. Let d_c be the distance between the base station and the intersection at which the mobile station makes a turn. Following [16], we introduce the dimensionless parameter x_0, the distance parameters x_L, y_0, y_L, and the exponents ξ, η, q. The corner effect results in a signal drop of ΔS dB in y_0 m. The log-normal shadowing processes before and after the mobile station makes a turn at the intersection are denoted by $10^{L_1(\mathbf{x},\mathbf{0})/10}$ and $10^{L_2(\mathbf{x},\mathbf{0})/10}$, respectively. The corner detection method of Section V will be evaluated for several values of the parameters introduced here. With these definitions, the average received power for a mobile station at position $\mathbf{x}$ is

$$p(\mathbf{x}, \mathbf{0}) = \begin{cases} P_0\left(\frac{\|\mathbf{x}\|}{x_0}\right)^{-2}\left[1+\left(\frac{\|\mathbf{x}\|}{x_L}\right)^{(\xi-2)q}\right]^{-1/q} 10^{L_1(\mathbf{x},\mathbf{0})/10}, \\ \qquad \mathbf{x} = [d_1 \quad 0]^T, \quad 0 < d_1 \le d_c \\ p([d_c \quad 0]^T, \mathbf{0}) 10^{-\Delta S\|\mathbf{x}-[d_c \quad 0]^T\|/(10y_0)}, \\ \qquad \mathbf{x} = [d_c \quad d_2]^T, \quad 0 < d_2 \le y_0 \\ p([d_c \quad y_0]^T, \mathbf{0})\left(\frac{\|\mathbf{x}-[d_c \quad 0]^T\|}{y_0}\right)^{-2} \\ \quad \times\left[1+\left(\frac{\|\mathbf{x}-[d_c \quad 0]^T\|}{y_L}\right)^{(\eta-2)q}\right]^{-1/q} 10^{L_2(\mathbf{x},\mathbf{0})/10}, \\ \qquad \mathbf{x} = [d_c \quad d_2]^T, \quad d_2 > y_0 \end{cases} \quad (9)$$

where the superscript ^{T} denotes the transpose operator and P_0 is a constant that accounts for transmitted power and antenna gains. As in Section II.A, the noiseless complex envelope $r_c(\mathbf{x})$ is generated by (3) using the average received power given in (9).

C. Noise Model

The noise model developed here is based on a receiver for a digital wireless system in which the received complex envelope is processed as follows. Baseband Gaussian noise $n_{\mathrm{BB}}(t)$ is added to the noiseless complex envelope. The bandwidth of $n_{\mathrm{BB}}(t)$ is $1/T$, where T is the symbol duration of the digitally modulated waveform. To reduce the effect of noise on the speed estimates, the signal is passed through a unit-gain, square-root raised cosine lowpass Doppler filter with bandwidth $f_D(1+\alpha)/(1-\alpha)$. The maximum Doppler frequency at the highest speed of interest is f_D, and the excess bandwidth factor is α with $0 < \alpha < 1$. Since f_D is on the order of a few hundred Hertz for terrestrial mobile wireless systems, an analog implementation of the Doppler filter may require off-chip discrete components. Alternatively, a digital raised cosine filter can be used. The Doppler filter frequency response is unity for $|f| \le f_D$. We define $T_D = (1-\alpha)/(2f_D)$ for use in Section IV. The output of the filter is $r(t)$. Let $w(t)$ denote the noise at the filter output. The in-phase and quadrature components of $w(t)$ each have variance σ_n^2.

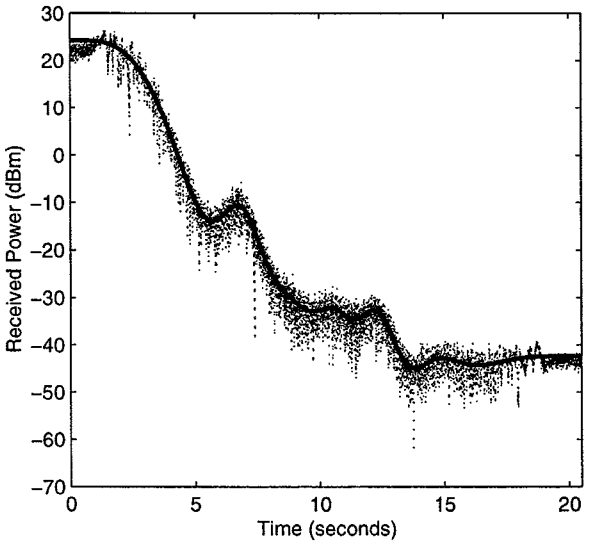

Fig. 1. Example of received signal for a variable mobile speed. Solid: true average received power; dotted: received multipath signal with additive noise and $\mathrm{SNR} = 20$ dB.

The curve Γ traversed by the mobile station is parametrized by the scalar position variable $x(t)$. Suppose that the mobile station travels along Γ with a speed $v(t)$ at time t. The filter output $r(t)$ is given by

$$r(t) = r_c(\Gamma[x(t)]) + w(t) \quad (10)$$

where $x(t) = \int_0^t v(t')\,dt'$ and the time origin is chosen such that $x(0) = 0$. An example of the received signal in a macrocellular environment is plotted in Fig. 1 for a variable mobile speed.

III. Estimation of Time-Varying Spectrum, Mobile Speed and Average Received Power

The signal $r_c(\mathbf{x})$ is locally stationary since the average received power $p(\mathbf{x}, \mathbf{x_B})$ varies slowly in space. Since (10) implies that $r_c(\mathbf{x})$ is mapped through the mobile speed to obtain $r(t)$, the signal $r(t)$ is also locally stationary. It is shown in [12] that there exists a basis of local cosine (or sine) functions that "almost diagonalizes" the covariance matrix of a locally stationary process. Reference [13] uses this fact to estimate the covariance of a locally stationary process from sampled data using

cosine packets. For the estimation of speed and average received power, local complex exponentials are needed in order to estimate the time-varying spectrum of the complex baseband signal $r(t)$. Tracking the variable mobile speed and average received power is accomplished using the time-varying spectrum. A description of the method is given in the following.

The signal $r(t)$ is sampled at rate $1/T_s$ to form $r[n]$. We process blocks of $r[n]$ and consider a typical block $r[n], n \in \{0, 1, \ldots, N-1\}$, where N is a dyadic length (power of two). Selection of a basis for diagonalization involves a recursive dyadic partition of the interval $I_{0,0} = \{0, 1, \ldots, N-1\}$ [17]. For each m satisfying $0 \le m \le M$, dyadic subintervals of $I_{0,0}$ with length $N2^{-m}$ are given by

$$I_{m,l} = \{N2^{-m}l, N2^{-m}l + 1, \ldots, N2^{-m}(l+1) - 1\}, \quad 0 \le l < 2^m. \quad (11)$$

The choice of M is discussed below. A recursive dyadic partition of $I_{0,0}$ is represented by $\mathcal{P}^\zeta = \{I_{m,l} : (m,l) \in \zeta\}$ where $I_{0,0} = \bigcup_{(m,l)\in\zeta} I_{m,l}$ and $I_{m,l} \bigcap I_{m',l'} = \emptyset$ for all $(m,l) \in \zeta, (m',l') \in \zeta, (m,l) \ne (m',l')$.

Associated with each subinterval $I_{m,l}$ are two smooth window functions $b_+^{m,l}[n]$ and $b_-^{m,l}[n]$. The window functions are nonzero over an interval consisting of $I_{m,l}$ extended by $\epsilon \in \mathbf{Z}^+$ samples at each endpoint. Smooth local exponential functions corresponding to $I_{m,l}$ are defined by

$$\begin{aligned}\Psi^{m,l,k}[n] = {} & b_+^{m,l}[n]\sqrt{\frac{1}{N2^{-m}}} \\ & \times \exp\left\{j\frac{2\pi k(n+1/2-N2^{-m}l)}{N2^{-m}}\right\} \\ & + b_-^{m,l}[n]\sqrt{\frac{1}{N2^{-m}}} \\ & \times \exp\left\{-j\frac{2\pi k(n+1/2-N2^{-m}l)}{N2^{-m}}\right\} \end{aligned} \quad (12)$$

where $-N2^{-m-1} \le k < N2^{-m-1}$. The window functions $b_+^{m,l}[n]$ and $b_-^{m,l}[n]$ are chosen such that if $M \le \log_2(N/(2\epsilon))$, then

$$B^\zeta = \{\Psi^{m,l,k}[n]\}_{(m,l)\in\zeta, -N2^{-m-1} \le k < N2^{-m-1}} \quad (13)$$

forms an orthonormal basis for discrete signals having compact support in $[\epsilon, N-\epsilon]$. The value of M is determined by the maximum acceptable uncertainty in frequency $(\Delta f)_{\max}$, i.e., $M = \lfloor \log_2(NT_s(\Delta f)_{\max}) \rfloor$. The ratio $||b_-^{m,l}||^2/(||b_+^{m,l}||^2 + ||b_-^{m,l}||^2)$ is kept small such that most of the energy of $\Psi^{m,l,k}[n]$ is contained in the first term of (12). The second term of (12) is needed to overcome the Balian-Low obstruction for orthonormal bases using windowed exponentials [18], [19]. The library of bases B^ζ that correspond to different recursive dyadic partitions of $I_{0,0}$ is denoted by $\mathcal{L}$.

We now consider $i_{\max}$ realizations of the received signal: $\{r_i[n]\}_{i\in\{1,\ldots,i_{\max}\}, n\in\{0,\ldots,N-1\}}$. A fast algorithm [19] based on the fast Fourier transform (FFT) is used to calculate the inner products $\langle \Psi^{m,l,k}, r_i \rangle = \sum_{n=0}^{N-1} \overline{\Psi^{m,l,k}[n]}\, r_i[n]$. A table of empirical variances $s^2_{m,l,k}$ is then calculated by

$$s^2_{m,l,k} = \frac{1}{i_{\max}} \sum_{i=1}^{i_{\max}} |\langle \Psi^{m,l,k}, r_i \rangle|^2, \quad \Psi^{m,l,k} \in B^\zeta. \quad (14)$$

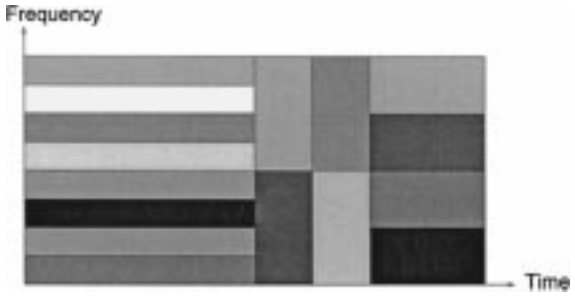

Fig. 2. Example of time-varying spectrum estimate. The grey level in each tile indicates relative power.

We wish to find a "best" basis $B^{\tilde{\zeta}}$ for covariance estimation of $r_i[n]$ among all the bases $\{B^\zeta\}_{\zeta\in\Lambda}$ in the library $\mathcal{L}$. The basis $B^{\tilde{\zeta}}$ is chosen to maximize the following convex functional of the empirical variances:

$$\begin{aligned}\sum_{(m,l)\in\tilde{\zeta}} \sum_{k=-N2^{-m-1}}^{N2^{-m-1}-1} \left(s^2_{m,l,k}\right)^2 \\ = \max_{\zeta\in\Lambda} \sum_{(m,l)\in\zeta} \sum_{k=-N2^{-m-1}}^{N2^{-m-1}-1} \left(s^2_{m,l,k}\right)^2. \end{aligned} \quad (15)$$

The best basis criterion (15) is equivalent to minimizing the Hilbert-Schmidt norm of the error in estimating the covariance matrix of $r_i[n]$ when the off-diagonal matrix elements are estimated by zero. The number of bases $B^\zeta \in \mathcal{L}$ is greater than $2^{2^{M-1}}$. However, there exists a fast dynamic programming algorithm [17] which selects the best orthonormal basis $B^{\tilde{\zeta}}$ in $O(N \log_2 N)$ operations. The computational complexity of this speed and average received power estimator is dominated by the number of operations required to compute $s^2_{m,l,k}$, which are computed in $O(i_{\max} N (\log_2 N)^2)$ operations. The best basis corresponds to a particular partitioning $\mathcal{P}^{\tilde{\zeta}}$ of the interval $I_{0,0}$. We obtain a coarse estimate of the time-varying spectrum by associating $s^2_{m,l,k}$ with the time-frequency tile $[NT_s2^{-m}l, NT_s2^{-m}(l+1)) \times [(k-1/2)/(NT_s2^{-m}), (k+1/2)/(NT_s2^{-m}))$ in the basis $B^{\tilde{\zeta}}$. The basis element $\Psi^{m,l,k}$ has most of its energy concentrated in this tile. Fig. 2 illustrates a time-varying spectrum estimate corresponding to a best basis partition $\mathcal{P}^{\tilde{\zeta}}$.

An estimate of the maximum Doppler frequency and, hence, the mobile speed are obtained using the time-varying spectrum. For mobile speed v and carrier wavelength λ, the maximum Doppler frequency $f_{\max}$ is $f_{\max} = v/\lambda$. In some propagation environments, there is no significant power incident at angles of 0 or π radians with respect to the mobile velocity. In such cases, the bandwidth of the time-varying spectrum is less than the maximum Doppler frequency. For robust estimation of the mobile speed and the average received power in these situations, the received complex envelopes from two antennas are used. The signals from the two antennas yield $i_{\max} = 2$ realizations: $r_1[n]$ and $r_2[n]$.

We consider the estimate of the time-varying spectrum for a subinterval $I_{m,l} \in \mathcal{P}^{\tilde{\zeta}}$. The estimates of the maximum Doppler frequency and the average received power are placed at the midpoint in time of the time-frequency tiles associated with

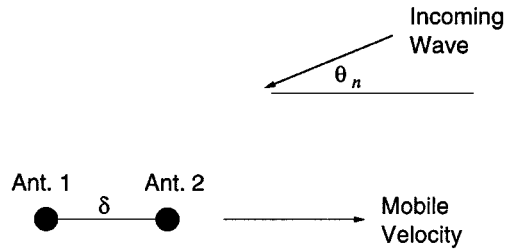

Fig. 3. Antenna geometry and angle of arrival of incoming wave (top view).

$I_{m,l}$, i.e., at time $t_0 = NT_s 2^{-m}(l+1/2)$. Let $\{c_n\}_{n=1,\ldots,n_{\max}}$ denote the local maxima of $\{s^2_{m,l,k}\}$ as k varies (m and l are fixed). The c_n's are sorted in decreasing order. The center frequency of the time-frequency tile that corresponds to c_n is $f_n = k_n/(NT_s 2^{-m})$. The Doppler frequency f_n of an incoming wave is related to its angle of arrival θ_n (with respect to the mobile velocity) by

$$f_n = f_{\max}\cos\theta_n. \tag{16}$$

The two-element antenna array is oriented along the mobile velocity to estimate the angles θ_n corresponding to the Doppler frequencies f_n. Fig. 3 illustrates the antenna geometry and relevant variables. The separation distance between the antenna elements is $\delta < \lambda/2$. The coefficients in the best basis expansion of the received complex envelopes for frequency f_n are related by

$$\langle \Psi^{m,l,k_n}, r_2\rangle \approx \langle \Psi^{m,l,k_n}, r_1\rangle \exp\{j\varsigma\cos\theta_n\} \tag{17}$$

where $\varsigma = 2\pi\delta/\lambda$. The approximation is due to the presence of noise and boundary effects. Therefore, an estimate for $\cos\theta_n$ is

$$\widehat{\cos\theta}_n = \frac{1}{\varsigma}[\arg(\langle \Psi^{m,l,k_n}, r_2\rangle) - \arg(\langle \Psi^{m,l,k_n}, r_1\rangle)]. \tag{18}$$

In order to separate the local maxima c_n that are due to noise from the local maxima that are due to the incoming signal, the following method is adopted. If $c_2/c_1 < \tau_1$, only the largest local maximum c_1 is declared to be due to signal. This situation would arise, for instance, when there is a line of sight between the base station and the mobile station. The selection of the threshold τ_1 is discussed in Section IV. From (16), the estimate of the maximum Doppler frequency at time t_0 for this case is

$$\hat{f}_{\max}(t_0) = \begin{cases} \left|\dfrac{f_1}{\widehat{\cos\theta}_1}\right|, & 0 < |\widehat{\cos\theta}_1| \le 1 \\ |f_1|, & \text{otherwise.} \end{cases} \tag{19}$$

If $c_2/c_1 \ge \tau_1$, we identify all local maxima $\{c_n\}_{n=1,2,\ldots,n_{\tau_2}}$ satisfying another threshold condition, i.e., $c_n/c_2 \ge \tau_2$ for $n = 1, 2, \ldots, n_{\tau_2}$ and $0 \le \tau_2 \le 1$. This condition is imposed to provide robustness to noise while accounting for a possible dominant multipath component (e.g., in Rician fading). The choice of τ_2 is also discussed in Section IV. An estimate of the maximum Doppler frequency for this case is given by

$$\hat{f}_{\max}(t_0) = \max\left\{|f_1|, \underset{\substack{n=1,2,\ldots,n_{\tau_2}\\ 0<|\widehat{\cos\theta_n}|\le 1}}{\text{median}} \left|\frac{f_n}{\widehat{\cos\theta_n}}\right|\right\}. \tag{20}$$

The median (instead of the mean) is used in (20) for robustness to outliers. The estimate of the mobile speed is then

$$\hat{v}(t_0) = \hat{f}_{\max}(t_0)\lambda. \tag{21}$$

Let $k_{\max}$ denote the index of the time-frequency tile with the largest center frequency less than or equal to $\hat{f}_{\max}(t_0)$, i.e.,

$$\hat{f}_{\max}(t_0) \ge |k/(NT_s 2^{-m})|, \quad 0 \le |k| \le k_{\max}. \tag{22}$$

The average received power is estimated by the integral in frequency of the time-varying spectrum for frequencies with absolute value less than or equal to $\hat{f}_{\max}(t_0)$. The estimate of the average received power at time t_0 is then given by

$$\hat{p}(t_0) = \frac{1}{N2^{-m+1}} \sum_{k=-k_{\max}}^{k_{\max}} s^2_{m,l,k}. \tag{23}$$

Estimates of the maximum Doppler frequency and the average received power are obtained in this manner for each of the subintervals of the best basis partition, $I_{m,l} \in \mathcal{P}^{\tilde{\zeta}}$. To limit estimation error, we discard speed and average power estimates that do not satisfy a maximum acceleration constraint. The following section describes the selection of the thresholds τ_1 and τ_2 and the block length N. Results of simulations that apply the speed and average power estimation technique are presented. The speed and average power estimators using best basis methods are also compared with an extension of the adaptive averaging method described in [3].

IV. Parameter Selection and Simulation Results

The threshold τ_1 is determined by considering a wide-sense stationary, line-of-sight propagation environment. In this case, the discrete-time noiseless complex envelope can be represented by

$$r[n] = \sqrt{2P_r}\exp\{j2\pi k_0 n/N\} \tag{24}$$

where P_r is the average power of $r[n]$ and $k_0 \in \{0, \ldots, N-1\}$. A unitary N-point discrete Fourier transform (DFT) of $r[n]$ yields

$$R[k] = \sqrt{2NP_r}\delta[k-k_0] \tag{25}$$

where $\delta[\cdot]$ denotes the Kronecker delta function. Therefore, the local maximum of the power spectrum of $r[n]$ is $\max_k\{E[|R[k]|^2]\} = \max_k |R[k]|^2 = 2NP_r$.

Let $W[k]$ denote a unitary N-point DFT of the discrete-time noise at the output of the Doppler filter. It can be shown that

$$\max_k\{E[|W[k]|^2]\} = 2\sigma_n^2 T_D/T_s. \tag{26}$$

In order to discard the local maxima due to noise, we require $\tau_1 > \max_k |W[k]|^2/\max_k |R[k]|^2$. Since (26) gives the maximum of the true noise power spectrum (instead of the empirical spectrum), a factor F is introduced for $\max_k |W[k]|^2$. Thus

$$\tau_1 > \frac{FT_D/T_s}{N\cdot \text{SNR}_p} \tag{27}$$

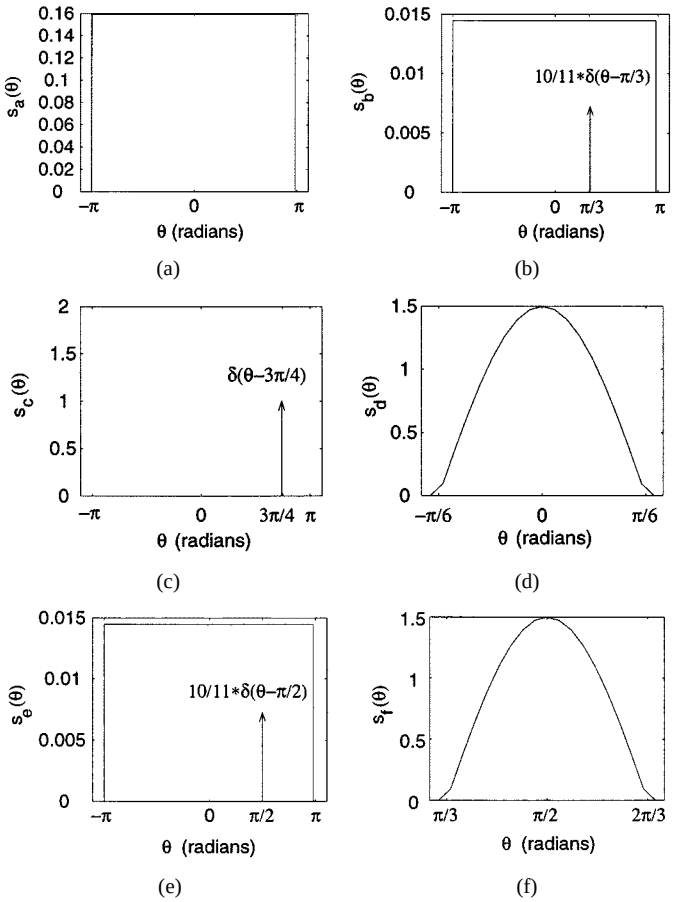

Fig. 4. Angular distributions of incident power used in simulations.

where $\mathrm{SNR}_p = P_r/\sigma_n^2$ is the processing signal-to-noise ratio (SNR). The SNR at the input of the Doppler filter must be at least 3–5 dB for synchronization and at least 8–10 dB for system operation. Typical maximum Doppler frequencies are less than 300 Hz, and typical signalling rates are greater than 30 kHz. Therefore, the Doppler filter introduces a gain of at least 20 dB in SNR, and hence, $\mathrm{SNR}_p \geq 20$ dB in the absence of frequency offset between the receiver and transmitter. For $F = 3, T_D/T_s = 5, N = 512$ and $\mathrm{SNR}_p = 20$ dB, (27) implies $\tau_1 > 3 \times 10^{-4}$. An upper bound for τ_1 is obtained by considering an angular distribution with a diffuse component and a discrete (specular) component (Rician fading). Let the angle of arrival of the discrete component be $\pi/2$ with respect to the direction of travel and the diffuse component be uniformly distributed in angle in a plane. This distribution represents a worst case since most of the power contributes to a Doppler frequency of 0 Hz. For a ratio of specular-to-diffuse power (Rice factor) of 10, $c_2/c_1 \approx 3 \times 10^{-3}$. Therefore, $\tau_1 < 3 \times 10^{-3}$ in order to estimate the speed for this distribution of incident power. These considerations lead to the choice $\tau_1 = 10^{-3}$.

The second threshold τ_2 is selected by simulations using six different angular distributions $s(\theta)$ of incident power. Plots of the various distributions used in the simulations are shown in Fig. 4, and brief descriptions are given in Table I. In order to select the threshold τ_2 independently of the mobile speed, spatial sampling at a constant interval is used. In addition, the average received signal power and noise power are kept constant

TABLE I
ANGULAR DISTRIBUTIONS OF INCIDENT POWER USED IN SIMULATIONS ($\delta(\cdot)$ DENOTES THE DIRAC DELTA FUNCTION)

Angular Distribution	Description
$s_a(\theta) = 1/(2\pi)\,\mathrm{rect}(\theta/(2\pi))$	Uniform Rayleigh Fading
$s_b(\theta) = (10/11)\,\delta(\theta - \pi/3) + 1/(22\pi)\,\mathrm{rect}(\theta/(2\pi))$	Rician Fading, Specular Comp. at $\pi/3$
$s_c(\theta) = \delta(\theta - 3\pi/4)$	Line of Sight at $3\pi/4$
$s_d(\theta) = 1.5\cos(3\theta)\,\mathrm{rect}(3\theta/\pi)$	Nonuniform Rayleigh Fading Near 0
$s_e(\theta) = (10/11)\,\delta(\theta - \pi/2) + 1/(22\pi)\,\mathrm{rect}(\theta/(2\pi))$	Rician Fading, Specular Comp. at $\pi/2$
$s_f(\theta) = 1.5\cos(3(\theta - \pi/2)) \times \mathrm{rect}(3(\theta - \pi/2)/\pi)$	Nonuniform Rayleigh Fading Near $\pi/2$

such that $\mathrm{SNR}_p = 20$ dB. For each angular distribution of incident power, 20 realizations are simulated, each having 50 speed and average power estimates (a total of 1000 speed and average power estimates per distribution). The separation distance between estimates is 51.2λ. This choice is motivated by the results of [8].

The normalized bias and mean square error (MSE) of the speed estimates are $E[\hat{v}/v - 1]$ and $E[(\hat{v}/v - 1)^2]$, respectively. Similarly, the normalized bias and MSE of the average power estimates are $E[\hat{p}/p - 1]$ and $E[(\hat{p}/p - 1)^2]$, respectively. For the angular distributions considered, Figs. 5 and 6 are plots of the normalized bias and MSE of the speed and average power estimates, respectively, as τ_2 is varied. The bias and MSE do not vary as a function of τ_2 for the line-of-sight distribution $s_c(\theta)$. This behavior is due to the fact that the local maxima, c_n, of the spectrum due to noise are discarded using the first threshold ($c_2/c_1 < \tau_1$); thus, the second threshold τ_2 is never used for this distribution. The negative biases in the speed estimates for $s_e(\theta)$ and $s_f(\theta)$ increase in magnitude with τ_2 since fewer local maxima of the spectrum are used to estimate the mobile speed, and most of the large local maxima for these distributions are concentrated near a Doppler frequency of 0 Hz. The relatively large magnitude bias and MSE in the average power estimates for $s_d(\theta)$ can be explained as follows. The mean distance between the local minima of the *squared envelope* $|r_c(\mathbf{x})|^2$ is around 13λ for $s_d(\theta)$. In contrast, the mean distance between the local minima of $|r_c(\mathbf{x})|^2$ for the other distributions (except for the line-of-sight case) is in the range $\lambda/2$–2λ. Thus, the averaging distance of 51.2λ does not completely remove the small-scale envelope variations present for $s_d(\theta)$, and the result is a large magnitude bias and MSE for the estimates of the average received power. In contrast, the correlation length of the *complex envelope* $r_c(\mathbf{x})$ for $s_d(\theta)$ is on the order of $\lambda/2$. Therefore, there is neither a large bias nor a large MSE for the speed estimates since a distance of 51.2λ contains several correlation lengths of the complex envelope, which is used to estimate the mobile speed. Figs. 5 and 6 indicate a desired value of the threshold $\tau_2 = 0.1$. The normalized bias and MSE of the speed and average power estimates are also investigated as SNR_p varies from 20 to 30 dB. No significant change in performance is observed for this range of SNR_p.

The choice of the block length N represents a trade-off between the delay in obtaining speed and average power estimates and the minimum detectable nonzero speed $v_{\min}$. For a block

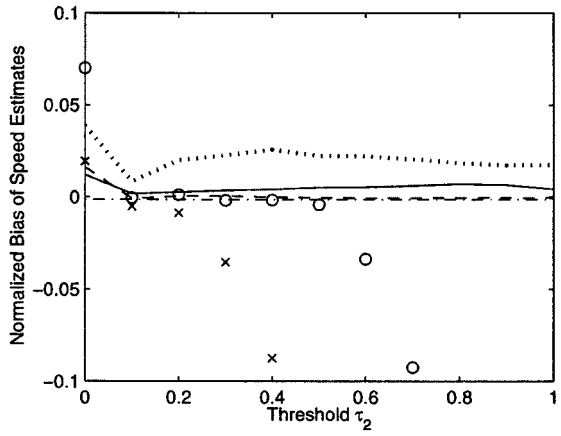

(a)

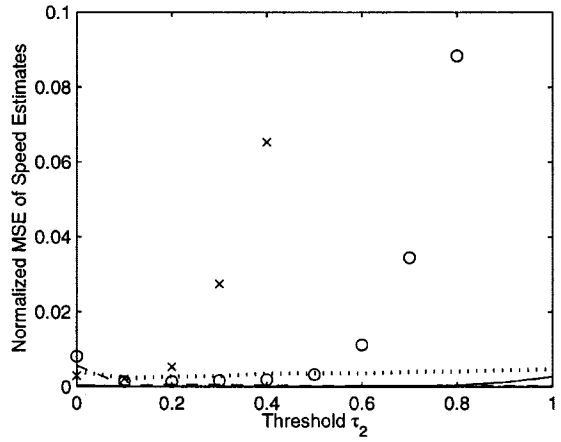

(b)

Fig. 5. (a) Normalized bias and (b) normalized mean square error of speed estimates as a function of threshold τ_2 for $\mathrm{SNR}_p = 20$ dB. Solid: $s_a(\theta)$; dotted: $s_b(\theta)$; dash-dot: $s_c(\theta)$; dashed: $s_d(\theta)$; 'x': $s_e(\theta)$; 'o': $s_f(\theta)$.

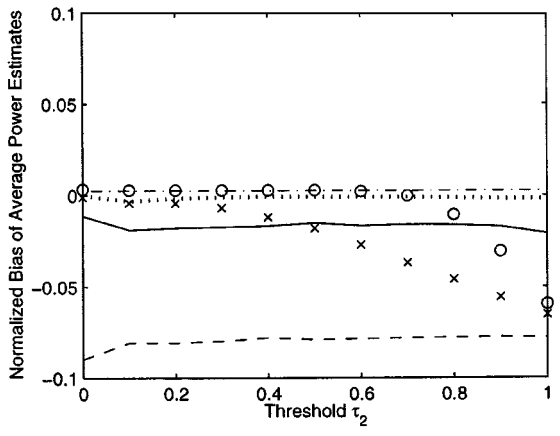

(a)

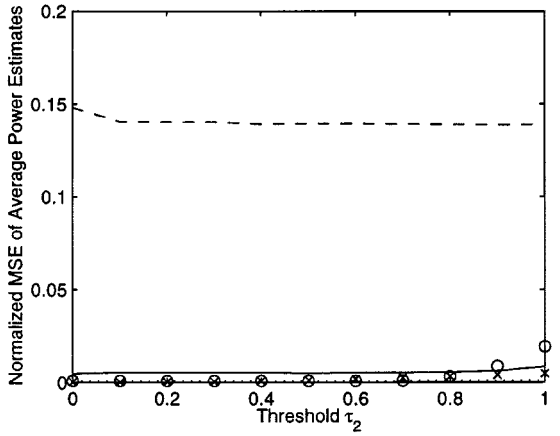

(b)

Fig. 6. (a) Normalized bias and (b) normalized mean square error of average power estimates as a function of threshold τ_2 for $\mathrm{SNR}_p = 20$ dB. Solid: $s_a(\theta)$; dotted: $s_b(\theta)$; dash-dot: $s_c(\theta)$; dashed: $s_d(\theta)$; 'x': $s_e(\theta)$; 'o': $s_f(\theta)$.

length of N and a sampling period of T_s, the time-frequency tile for the root interval $I_{0,0}$ has a height of $1/(NT_s)$. Therefore, the minimum detectable nonzero speed is

$$v_{\min} = \frac{\lambda}{2NT_s}. \tag{28}$$

Numerical values of N for speed tracking and corner detection are given below.

In order to demonstrate the tracking of changes in mobile speed, the speed and average power estimators are applied to the following speed profile $v(t)$, [$v(t)$ is in kilometers per hour (km/h) and t in seconds]:

$$v(t) = \begin{cases} 0, & 0 \le t < 0.5 \\ 100\Upsilon\left(\frac{t-0.5}{8}\right), & 0.5 \le t < 8.5 \\ 100, & 8.5 \le t < 11.5 \\ 100\Upsilon\left(\frac{19.5-t}{8}\right), & 11.5 \le t < 19.5 \\ 0, & 19.5 \le t \le 20 \end{cases} \tag{29}$$

where

$$\Upsilon(t) = \begin{cases} 0, & t < 0 \\ 3t^2 - 2t^3, & 0 \le t < 1 \\ 1, & 1 \le t. \end{cases} \tag{30}$$

For purposes of comparison, the adaptive averaging method of [3] has been extended to account for angular distributions other than uniform Rayleigh fading. In this method, the following quantities are computed at time index n:

$$\begin{aligned} S_n &= \kappa_{n-1}|r[n]|^2 + (1-\kappa_{n-1})S_{n-1} \\ R_n &= \kappa_{n-1}|r[n]|^4 + (1-\kappa_{n-1})R_{n-1} \\ V_n &= \kappa_{n-1}(|r[n]|^2 - |r[n-1]|^2)^2 + (1-\kappa_{n-1})V_{n-1} \\ \hat{f}_{\max,n} &= \frac{1}{2\pi T_s}\sqrt{\frac{V_n}{R_n - S_n^2}} \\ N_{\mathrm{av},n} &= \left\lfloor \frac{d_{\mathrm{av}}}{\lambda T_s \hat{f}_{\max,n}} + 0.5 \right\rfloor \\ \kappa_n &= \frac{1}{N_{\mathrm{av},n}+1}. \end{aligned} \tag{31}$$

The estimates of the maximum Doppler frequency and the average received power at time index n are given by $\hat{f}_{\max,n}$ and $S_n/2$, respectively. The averaging interval $N_{\mathrm{av},n}$ is adapted to achieve a target averaging distance of $d_{\mathrm{av}} = 20\lambda$, in accordance with the results given in [8].

Fig. 7 is a plot of the speed $v(t)$ and the speed estimates using the best basis and the adaptive averaging methods for the angular distribution $s_b(\theta)$ and $\mathrm{SNR}_p = 20$ dB. For the best basis

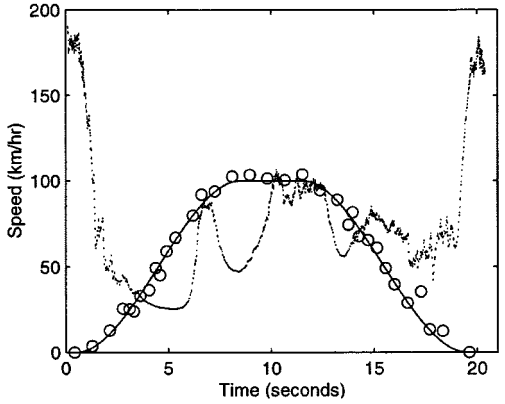

Fig. 7. Tracking performance of speed estimators for angular distribution $s_b(\theta)$ and $\mathrm{SNR}_p = 20$ dB. Solid: true mobile speed; 'o': speed estimates using best basis method; dotted: speed estimates using adaptive averaging method.

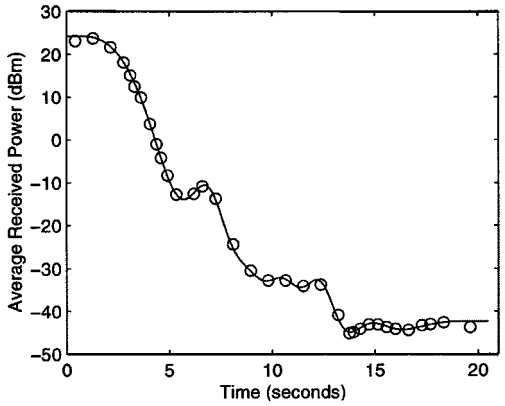

Fig. 8. Tracking performance of average power estimator for angular distribution $s_b(\theta)$ and $\mathrm{SNR}_p = 20$ dB. Solid: true average received power; 'o': average power estimates using best basis method.

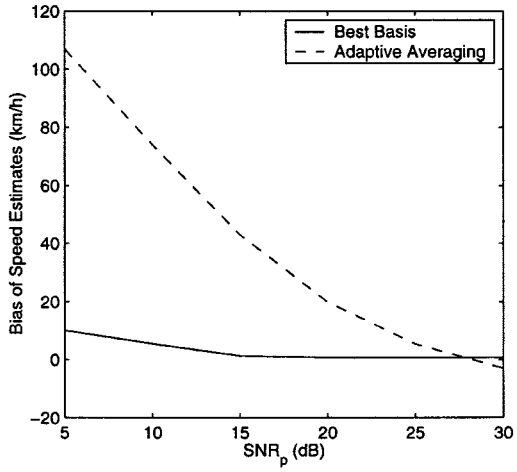

(a)

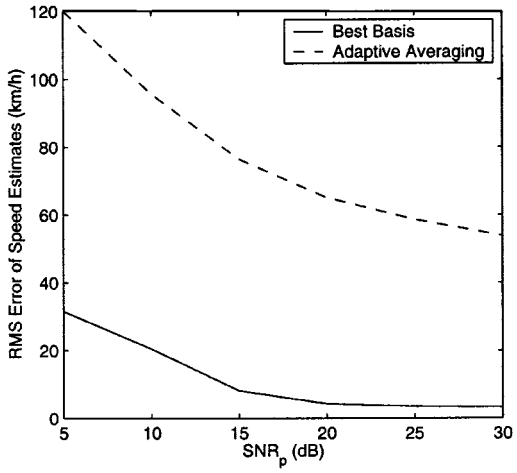

(b)

Fig. 9. (a) Bias and (b) root mean square error of speed estimates versus SNR_p for speed profile (29) and angular distribution $s_b(\theta)$.

method, estimates which imply an acceleration with absolute value greater than $2g$ are discarded ($g \approx 9.8$ m/s^2 is the acceleration due to gravity). The duration of each signal block used in this example is 1.706 s with $N = 4096$ samples ($v_{\min} = 0.35$ km/h). The maximum uncertainty in frequency is $(\Delta f)_{\max} = 5$ Hz, the carrier wavelength is $\lambda = 1/3$ m, the correlation length of the log-normal shadowing is $d_0(\mathbf{x_B}) = 50$ m, and the exponent of distance dependence is $\gamma = 4$.

It can be seen in Fig. 7 that the adaptive averaging method is unable to track the variable mobile speed. The large estimation error of the adaptive averaging method for low mobile speed is due to the rapid variations in the signal envelope caused by additive noise. Fig. 8 is a plot of the corresponding average received power (in dBm) and the average power estimates using the best basis method. The average power estimates using the adaptive averaging method are not shown since the performance is similar to that of the best basis method. The results show that in contrast to the adaptive averaging method, the best basis method is able to track variable mobile speeds well.

The performances of the best basis and adaptive averaging methods for speed profile (29) as a function of SNR_p are compared in Figs. 9 and 10. The results are presented for angular distribution $s_b(\theta)$ and represent averages over 100 realizations of the fading process. Values of SNR_p less than 20 dB may occur in practice due to a frequency offset between the receiver and transmitter. From Fig. 9(a) and (b), the best basis method for estimating the mobile speed performs significantly better than the adaptive averaging method, in agreement with the results given in Fig. 7. Fig. 10(a) and (b) indicate that the two methods have similar performance for estimating the average received power. The results for variable speeds demonstrate that the best basis method performs significantly better than the adaptive averaging method for the range of SNR_p encountered in practice.

V. Corner Detection Method

This section describes a method to detect the corner effect in urban propagation environments. The detection method is evaluated using the propagation model of Section II-B. The corner detection method uses the speed and average power estimates obtained as described in Section III, except that there is no maximum acceleration constraint on the speed estimates in order to reduce the detection delay. The current and past speed estimate samples are linearly interpolated to the rate $1/T_s$. A similar interpolation is performed for the average power estimates expressed in dBm. An estimate of the distance traveled by the mobile station is obtained from the integral of the interpolated

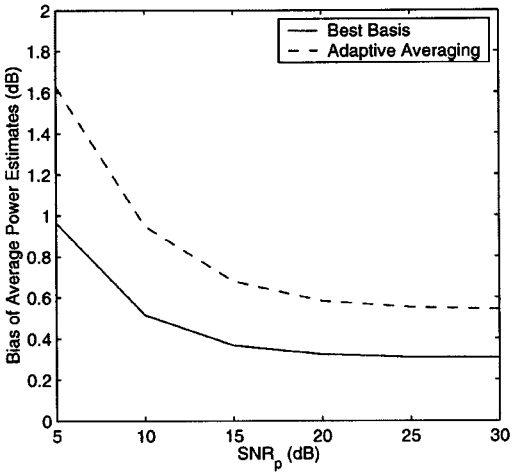

(a)

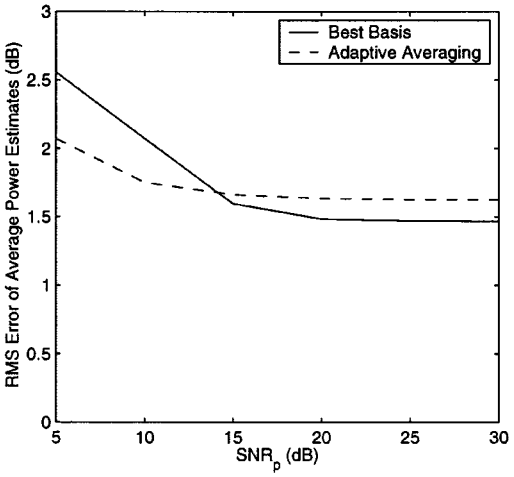

(b)

Fig. 10. (a) Bias and (b) root mean square error of average received power estimates versus SNR_p for speed profile (29) and angular distribution $s_b(\theta)$.

TABLE II
MICROCELLULAR PROPAGATION PARAMETERS FOR CORNER DETECTION.

x_0	x_L (m)	y_0 (m)	y_L (m)	ξ	η
1.0	189	1.5	180	4.6	5.1
1.4	408	3.0	110	8.3	3.5
0.5	95	4.0	100	4.0	3.0

speed estimates. The corner effect is detected if the average power changes by at least H_c dB in the last y_c m. If the intersections in a city are separated by ΔY m, the mobile station must travel at least ΔY m before another corner is detected.

The corner detection algorithm is evaluated for various microcellular propagation parameters. Table II lists three sets of values for the parameters used in (9). These values are based on the empirical results of [16]. For each row of parameters in Table II, values of 15 and 20 dB for the corner signal drop ΔS are used. This drop occurs in a distance of y_0. The value of the exponent parameter q is chosen to be 4, the distance between the base station and the intersection is $d_c = 100$ m, and the minimum distance between intersections is $\Delta Y = 50$ m. The standard deviations for the log-normal shadowing before and after the mobile station makes a turn at the intersection are 4 and 7 dB, respectively, and the corresponding angular distributions of incident power ($s_1(\theta)$ and $s_2(\theta)$) are plotted in Fig. 11.

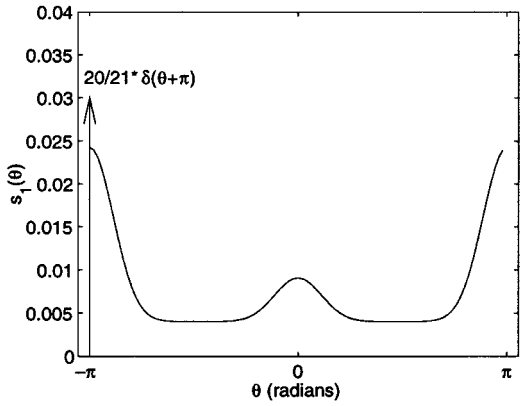

(a)

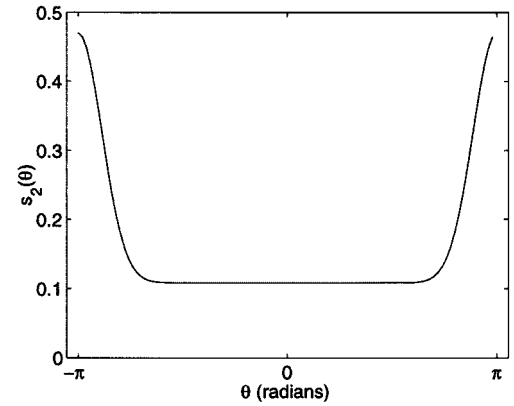

(b)

Fig. 11. Angular distribution of incident power (a) before $(s_1(\theta))$ and (b) after $(s_2(\theta))$ mobile station makes turn at intersection.

The corner detection method is evaluated using two realistic speed profiles which capture the effects of slowing down $(v_1(t))$ and stopping $(v_2(t))$ when making a turn. The general form of the mobile speed near the intersection is given by

$$v_i(t) = \begin{cases} v_L + (v_H - v_L)\Upsilon\left(\frac{4-t}{4}\right), & 0 \le t < 4 \\ v_L, & 4 \le t < 6 \\ v_L + (v_H - v_L)\Upsilon\left(\frac{t-6}{4}\right), & 6 \le t \le 10 \end{cases} \quad (32)$$

where $i = 1, 2$ and $\Upsilon(\cdot)$ is defined in (30). The start of the signal drop ΔS occurs at $t = 6$ s. For both $v_1(t)$ and $v_2(t), v_H = 50$ km/h. For $v_1(t), v_L = 20$ km/h and for $v_2(t), v_L = 0$ km/h. For each set of propagation parameters, ten realizations of the received signal are simulated, yielding a total of 60 realizations for each speed profile. The delay in detection is defined to be the distance from the position of the start of the signal drop ΔS to the position of the mobile station when the corner is detected. This definition includes the delay due to the block processing of the received signal. The duration of each signal block used in the simulations is 0.427 s with $N = 1024$ samples. The corresponding minimum detectable nonzero speed is $v_{\min} = 1.4$ km/h.

Tables III and IV summarize the results of the corner detection algorithm for speed profiles $v_1(t)$ and $v_2(t)$. The threshold

TABLE III
CORNER DETECTOR PERFORMANCE FOR SPEED PROFILE $v_1(t)$.

H_c (dB)	False Alarms	Missed Detections	Mean Detection Delay (m)
3	24	0	2.40
4	5	0	2.87
5	0	0	3.64
6	0	1	4.19
7	0	1	4.78
8	0	4	4.16
9	0	5	4.19
10	0	9	4.31

TABLE IV
CORNER DETECTOR PERFORMANCE FOR SPEED PROFILE $v_2(t)$.

H_c (dB)	False Alarms	Missed Detections	Mean Detection Delay (m)
3	23	0	1.39
4	9	0	1.77
5	0	0	2.13
6	0	1	2.40
7	0	1	2.76
8	0	2	2.94
9	0	7	2.98
10	0	9	3.25

H_c is varied for $y_c = 3$ m. The mean detection delays given in Tables III and IV are determined excluding the false alarms and the missed detections. The results indicate that for $H_c \leq 4$ dB, there is a significant number of false alarms since, at very low thresholds H_c, the shadowing is mistaken for a corner. Furthermore, for $H_c \geq 6$ dB, some corners are not detected. Therefore, for the microcellular propagation environments considered here, a desired value for the threshold H_c is $H_c \approx 5$ dB. The corresponding mean delays are 3.64 m and 2.13 m for speed profiles $v_1(t)$ and $v_2(t)$, respectively.

Another corner detection algorithm is described in [20] where the assumptions of constant mobile speed and spatial sampling of the signal are made. While it is desirable to compare the two corner detection methods, the ideal assumptions of [20] make the comparison difficult. The method described here is seen to be effective in detecting the corner effect with small delay.

VI. EXTENSION: ARBITRARY ORIENTATION OF ANTENNAS

This section describes an extension of the speed and average power estimation method of Section III to account for arbitrary antenna orientations that are present for hand-held mobile stations. Since the antenna orientation is unknown, three antennas at the mobile station are needed. The antennas are arranged in a triangle; therefore, $i_{\max} = 3$ realizations of the complex envelope are used to estimate the time-varying Doppler power spectrum. Details of the method are discussed in the following.

Fig. 12 provides a top view of the three antennas arranged in an equilateral triangle. As in Section III, the antenna spacing is $\delta < \lambda/2$ and $\varsigma = 2\pi\delta/\lambda$. The arbitrary angle between the mobile velocity and the vector from Antenna 1 to Antenna 2 is ψ. The angle between Antennas 1 and 2 and Antennas 1 and 3

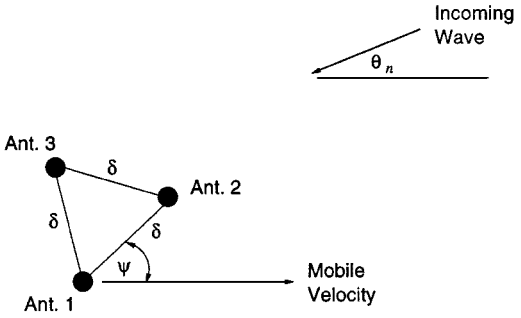

Fig. 12. Antenna geometry for three-antenna case (top view).

is $\beta = \pi/3$. We now consider two multipath waves incident at angles $\pm\theta_n$ with respect to the mobile velocity. These waves induce the same baseband Doppler frequency $f_n = f_{\max}\cos\theta_n$, where $f_{\max}$ is the unknown maximum Doppler frequency. Let $r_{1,n} = \langle \Psi^{m,l,k_n}, r_1 \rangle = a_n + b_n$ denote the coefficient in the best basis expansion of the complex envelope received at Antenna 1 for subinterval $I_{m,l}$ and for frequency f_n. Here, a_n and b_n are the complex amplitudes of the waves incident at θ_n and $-\theta_n$, respectively, and k_n is the frequency index corresponding to f_n. The coefficients corresponding to the complex envelopes received at Antennas 2 and 3 are denoted by $r_{2,n}$ and $r_{3,n}$, respectively. The following equations can be written for $f_n, r_{1,n}, r_{2,n}$, and $r_{3,n}$:

$$f_n = f_{\max}\cos\theta_n \tag{33}$$

$$r_{1,n} = a_n + b_n \tag{34}$$

$$r_{2,n} = a_n e^{j\varsigma\cos(\theta_n - \psi)} + b_n e^{j\varsigma\cos(\theta_n + \psi)} \tag{35}$$

$$r_{3,n} = a_n e^{j\varsigma\cos(\theta_n - \psi - \beta)} + b_n e^{j\varsigma\cos(\theta_n + \psi + \beta)}. \tag{36}$$

The equations given above are valid for a negligible frequency offset between receiver and transmitter and for far field conditions such that the magnitudes of a_n and b_n do not change significantly for the different antennas.

The five unknowns in (33)–(36) are $f_{\max}, a_n, b_n, \theta_n$, and ψ. Thus, the solution of these equations requires two frequencies f_n and f_m to obtain a total of eight equations in eight unknowns. These equations are independent for $|f_n| \neq |f_m|$. The equations can be solved by eliminating a_n and b_n for frequency f_n and by eliminating a_m and b_m for frequency f_m. Finally, from (33), the system of eight equations reduces to the following three equations:

$$\begin{aligned} &e^{j\varsigma\cos\theta_n[\cos(\psi+\beta)-\cos\psi]}\sin(\varsigma\sin\theta_n\sin(\psi+\beta)) \\ &\quad\times(r_{2,n} - r_{1,n}e^{j\varsigma\cos(\theta_n+\psi)}) - \sin(\varsigma\sin\theta_n\sin\psi) \\ &\quad\times(r_{3,n} - r_{1,n}e^{j\varsigma\cos(\theta_n+\psi+\beta)}) = 0 \end{aligned} \tag{37}$$

$$\begin{aligned} &e^{j\varsigma\cos\theta_m[\cos(\psi+\beta)-\cos\psi]}\sin(\varsigma\sin\theta_m\sin(\psi+\beta)) \\ &\quad\times(r_{2,m} - r_{1,m}e^{j\varsigma\cos(\theta_m+\psi)}) - \sin(\varsigma\sin\theta_m\sin\psi) \\ &\quad\times(r_{3,m} - r_{1,m}e^{j\varsigma\cos(\theta_m+\psi+\beta)}) = 0 \end{aligned} \tag{38}$$

$$f_n\cos\theta_m - f_m\cos\theta_n = 0. \tag{39}$$

The nonlinear system (37)–(39) can be written in the compact notation

$$\mathbf{F}(\mathbf{V}) = \mathbf{0} \tag{40}$$

where $\mathbf{V} = [V_1\ V_2\ V_3]^T = [\theta_n\ \theta_m\ \psi]^T$ and $\mathbf{F} = [F_1\ F_2\ F_3]^T$ is the vector-valued function representing the left hand sides of (37)–(39). Newton's method is used to solve the nonlinear system (40). Given an initial guess $\mathbf{V}_0$ and the matrix of first partials

$$D_{\mathbf{F}}(\mathbf{V}) = \left(\frac{\partial F_i}{\partial V_j}\right)_{i,j=1,2,3} \tag{41}$$

the solution for $\mathbf{V}$ is determined by iteration:

$$\mathbf{V}_{i+1} = \mathbf{V}_i - D_{\mathbf{F}}^{-1}(\mathbf{V}_i)\mathbf{F}(\mathbf{V}_i), \quad i = 0, 1, 2, \ldots \tag{42}$$

The iteration continues until a maximum iteration count is reached, the matrix $D_{\mathbf{F}}(\mathbf{V}_i)$ becomes ill conditioned, or

$$\frac{\|\mathbf{V}_{i+1} - \mathbf{V}_i\|}{\|\mathbf{V}_i\|} < \epsilon \tag{43}$$

for some small $\epsilon > 0$. The initial guess $\mathbf{V}_0 = [\theta_n^{(0)}\ \theta_m^{(0)}\ \psi^{(0)}]^T$ is determined as follows. For $|f_n| > |f_m|$,

$$\theta_n^{(0)} = \begin{cases} \pi/4, & f_n \geq 0 \\ 3\pi/4, & f_n < 0 \end{cases} \tag{44}$$

and $\theta_m^{(0)} = \cos^{-1}(f_m \cos\theta_n^{(0)}/f_n)$. For $|f_n| < |f_m|$, the roles of m and n are interchanged. The value for $\psi^{(0)}$ is varied in the interval $[-\pi, \pi)$ in steps of $\pi/4$. An estimate of $f_{\max}$ is obtained from the solution $\mathbf{V}$ using (33). Initial guesses which yield a large imaginary part for $\mathbf{V}$ or negative values for $f_{\max}$ are discarded.

Multiple estimates of $f_{\max}$ are obtained using pairs of frequencies (f_n, f_m) for which the corresponding local maxima (c_n, c_m) of the time-varying Doppler spectrum satisfy the threshold conditions discussed in Section III, i.e., $c_2/c_1 \geq \tau_1, c_n/c_2 \geq \tau_2, c_m/c_2 \geq \tau_2$. As in Section III, the median of the estimates of $f_{\max}$ is taken. The average received power is then estimated using (23). For the case $c_2/c_1 < \tau_1$, the frequency f_1 of the largest local maximum, c_1, is used as an estimate of $f_{\max}$. Thus, if the time-varying spectrum has at least two significant local maxima, this method provides robust estimates of the mobile speed and the average received power for arbitrary orientations of the mobile station antennas. If the frequency offset between receiver and transmitter is not negligible, $f_{\max}$ and the unknown frequency offset can be estimated using three significant local maxima in the Doppler power spectrum.

The threshold $\tau_1 = 10^{-3}$ is selected using the arguments given in Section IV. The threshold τ_2 is determined by simulations using the angular distributions of Table I and five different antenna orientations: $\psi \in \{0, \pi/6, \pi/4, \pi/3, \pi/2\}$. A value of $\tau_2 = 0.1$ is chosen using the normalized bias and MSE of the speed and average power estimates.

Fig. 13 is a plot of the estimates of the variable mobile speed (29) and the average received power (in dBm) for the angular distribution $s_b(\theta), \psi = \pi/4$, and $\mathrm{SNR}_p = 20$ dB. The results demonstrate good tracking performance. The corner detection method of Section V is evaluated using the speed and average power estimation technique for arbitrary antenna orientation as described here. For each speed profile ($v_1(t)$ and $v_2(t)$) and for each of the propagation environments used Section V, five orientations of the antennas are simulated: $\psi \in \{0, \pi/6, \pi/4, \pi/3, \pi/2\}$. The performance of the corner detection method is similar to the results given in Tables III and IV.

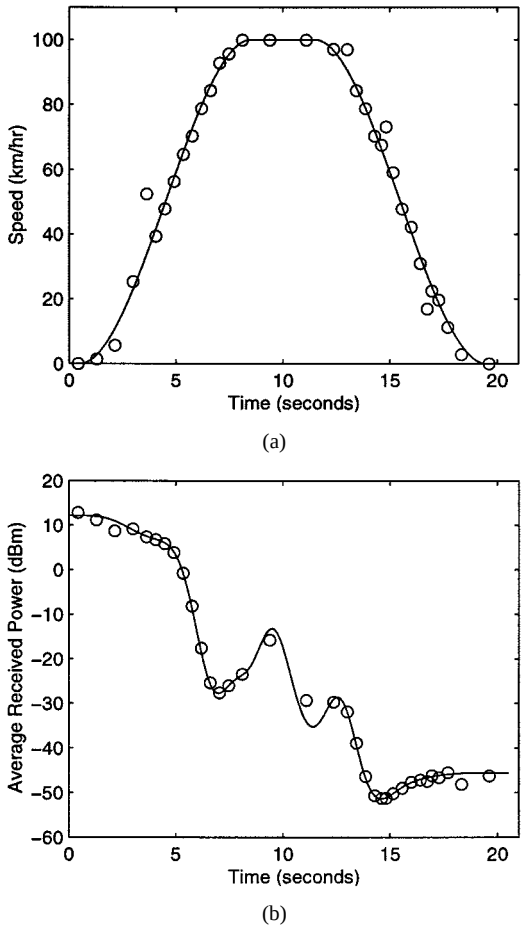

Fig. 13. Tracking performance of (a) mobile speed and (b) average power estimators for arbitrary antenna orientation, angular distribution $s_b(\theta)$, and $\mathrm{SNR}_p = 20$ dB. Solid: true mobile speed and average received power; 'o': speed and average power estimates using best basis method. Antenna orientation $\psi = \pi/4$.

VII. Conclusion

A new technique is described for estimating the mobile speed and the average received power in general wireless environments. The method uses the local stationarity of the received signal to expand the signal in a basis of smooth local exponential functions. The coefficients of the expansion provide an estimate of the time-varying Doppler power spectrum. The time-varying spectrum and a two-element antenna array are used to estimate and track the variable mobile speed and the average received power. This estimation method is extended to the case of an unknown, arbitrary orientation of the antennas at the mobile station. Using three antennas, this estimator is shown to yield

performance comparable to the method using two antennas oriented along the mobile velocity. The best basis estimator has been shown to perform significantly better than an extended adaptive averaging method.

The above technique is used to detect the corner effect present in urban cellular systems. A corner is detected if the average received power changes by a significant amount within a short distance. Simulations demonstrate that this method detects corners with small delay and, hence, is useful in reducing handoff delay and the call dropping rate.

REFERENCES

[1] W. C. Jakes, *Microwave Mobile Communications.* New York: Wiley, 1974.

[2] M. D. Austin and G. L. Stüber, "Velocity adaptive handoff algorithms for microcellular systems," *IEEE Trans. Veh. Technol.*, vol. 43, pp. 549–561, Aug. 1994.

[3] J. M. Holtzman and A. Sampath, "Adaptive averaging methodology for handoffs in cellular systems," *IEEE Trans. Veh. Technol.*, vol. 44, pp. 59–66, Feb. 1995.

[4] M. D. Austin and G. L. Stüber, "Eigen-based Doppler estimation for differentially coherent CPM," *IEEE Trans. Veh. Technol.*, vol. 43, pp. 781–85, Aug. 1994.

[5] J. Lin and J. G. Proakis, "A parametric method for Doppler spectrum estimation in mobile radio channels," in *Proc. 27th Ann. Conf. Info. Sci. Syst.*. Baltimore, MD, Mar. 25–27, 1993.

[6] M. Hellebrandt, R. Mathar, and M. Scheibenbogen, "Estimating position and velocity of mobiles in a cellular radio network," *IEEE Trans. Veh. Technol.*, vol. 46, pp. 65–71, Feb. 1997.

[7] A. J. Goldsmith, L. J. Greenstein, and G. J. Foschini, "Error statistics of real-time power measurements in cellular channels with multipath and shadowing," *IEEE Trans. Veh. Technol.*, vol. 43, pp. 439–446, Aug. 1994.

[8] W. C. Y. Lee, "Estimate of local average power of a mobile radio signal," *IEEE Trans. Veh. Technol.*, vol. VT-34, pp. 22–27, Feb. 1985.

[9] D. Wong and D. C. Cox, "An optimal local mean signal power level estimator for Rayleigh fading environments," in *Proc. Int. Conf. on Info., Commun. Signal Processing*, 1997, pp. 1701–1704.

[10] R. Narasimhan and D. C. Cox, "Speed estimation in wireless systems using wavelets," *IEEE Trans. Commun.*, vol. 47, no. 9, pp. 1357–1364, 1999.

[11] ——, "Wavelet-based estimation of the nonstationary mean signal in wireless systems," *IEEE J. Select. Areas Commun.*, vol. 18, pp. 2220–2226, Nov. 2000.

[12] S. Mallat, G. Papanicolaou, and Z. Zhang, "Adaptive covariance estimation of locally stationary processes," *Ann. Statist.*, vol. 26, no. 1, pp. 1–47, 1998.

[13] D. L. Donoho, S. Mallat, and R. von Sachs, "Estimating covariances of locally stationary processes: Consistency of best basis methods,", unpublished.

[14] D. C. Cox, "Universal digital portable radio communication," *Proc. IEEE*, vol. 75, no. 4, pp. 436–477, 1987.

[15] M. Gudmundson, "Correlation model for shadow fading in mobile radio systems," *Electron. Lett.*, vol. 27, no. 23, pp. 2145–2146, 1991.

[16] J.-E. Berg, R. Bownds, and F. Lotse, "Path loss and fading models for microcells at 900 MHz," in *Proc. IEEE Veh. Technol. Conf.*, 1992, pp. 666–671.

[17] R. Coifman and M. V. Wickerhauser, "Entropy based algorithms for best basis selection," *IEEE Trans. Inform. Theory*, vol. 32, pp. 712–718, 1992.

[18] I. Daubechies, "Ten lectures on wavelets," *SIAM CBMS-NSF Series in Appl. Math.*, 1992.

[19] M. V. Wickerhauser, *Adapted Wavelet Analysis from Theory to Software*. Wellesley, MA: A.K. Peters, 1994.

[20] M. D. Austin and G. L. Stüber, "Velocity adaptive handoff algorithms for microcellular systems," in *Proc. Int. Conf. on Univ. Pers. Commun.*, 1993, pp. 793–797.

Ravi Narasimhan (S'96–M'99) received the B.S. degree (with highest honors) in electrical engineering, the Certificate of Distinction from the Univerity of California at Berkeley in 1995, and the M.S. and Ph.D. degrees in electrical engineering from Stanford University in 1996 and 2000, respectively.

He is presently at Marvell Semiconductor, Inc., Sunnyvale, CA.His research interests includ wireless communication, signal processing, and wavelet analysis.

Dr. Narasimhan is a member of Phi Beta Kappa and Golden Key National Honor Society. He received the Warren Y. Dere Memorial Prize from the University of California at Berkeely in 1995. He secured the first rank in the Ph.D. qualifying examination in electrical engineering at Stanford University. He also rceived the Best Student Paper Award for U.S. at the IEEE Interenational Symposium on Personal, Indoor, and Mobile Radio Communications (PIMRC), held in Boston, MA, September 1998.

Donald C. Cox (S'58–M'61–SM'72–F'79) received the B.S. and M.S. degrees in electrical engineering from the University of Nebraska in 1959 and 1960, respectively, and the Ph.D. degree in electrical engineering from Stanford University in 1968. He received an Honorary Doctor of Science from the University of Nebraska in 1983.

From 1960 to 1963, he worked on microwave communications system design at Wright-Patterson AFB, OH. From 1963 to 1968 he was at Stanford University working on tunnel diode amplifier design and research on microwave propagat ion in the troposphere. From 1968 to 1973 his research at Bell Laboratories, Holmdel, NJ, in mobile radio propagation and on high-capacity mobile radio systems provided important input to early cellular mobile radio system development, and is continuing to contribute to the evolution of digital cellular radio, wireless personal communications systems and cordless telephones. From 1973 to 1983 he was Supervisor of a group at Bell Laboratories that did innovative propagation and system research for millimeter-wave satellite communications. In 1978 he pioneered radio system and propagation research for low-power wireless personal communications systems. At Bell Laboratories in 1983 he organized and became Head of the Radio and Satellite Systems Research Department that became a Division in Bell Communications Research (Bellcore) with the breakup of the Bell System on January 1, 1984. He was Division Manager of that Radio Research Division until it again became a department in 1991. He continued as Executive Director of the Radio Research Department where he championed, led and contributed to research on all aspects of low-power wireless personal communications entitled Universal Digital Portable Communications (UDPC). He was instrumental in evolving the extensive research results into specifications that became the U.S. Standard for the Wireless or Personal Access Communications System (WACS or PACS). In September 1983 he became a Professor of Electrical Engineering and Director of the Center for Telecommunications at Stanford University where he continues to pursue research and teaching of wireless mobile and personal communications. He was appointed Harald Trap Friis Professor of Engineering in 1994. He is author or coauthor of many papers and conference presentations, including many invited and several keynote addresses, and books. He has been granted 15 patents.

Dr. Cox was a member of the Administrative Committee of the IEEE Antennas and Propagation Society (1986–1988), an Associate Editor of the IEEE TRANSACTIONS ON ANTENNAS AND PROPAGATION (1983–1986), is a member of the National Academy of Engineering, is a member of Commissions B, C and F and USNC/URSI, and was a member of the URSI Intercommission Group on Time Domain Waveform Measurements (1982–1984). He was awarded the IEEE 1993 Alexander Graham Bell Medal "For pioneering and leadership in personal portable communications"; was a corecipient of the 1983 International Marconi Prize in Electromagnetic Wave Propagation (Italy); received the IEEE 1985 Morris E. Leeds award and the IEEE Third Millennium Medal in 2000; and received the 1983 IEEE Vehicular Technology Society paper of the year award, and the IEEE Communications Society 1992 L. G. Abraham Prize Paper Award and 1990 Communications Magazine Prize Paper Award. He received the Bellcore Fellow Award in 1991. He is a fellow of AAAS and the Radio Club of America. He is a member of Sigma Xi, Sigma Tau, Eta Kappa Nu and Phi Mu Epsilon, and is a Registered Professional Engineer in Ohio and Nebraska.